



**HAL**  
open science

## Optimisation of fast quantification of fluorine content using handheld laser induced breakdown spectroscopy

Y. Foucaud, C. Fabre, B. Demeusy, I.V. Filippova, L.O. Filippov

► **To cite this version:**

Y. Foucaud, C. Fabre, B. Demeusy, I.V. Filippova, L.O. Filippov. Optimisation of fast quantification of fluorine content using handheld laser induced breakdown spectroscopy. *Spectrochimica Acta Part B: Atomic Spectroscopy*, 2019, 158, pp.105628 -. 10.1016/j.sab.2019.05.017 . hal-03484488

**HAL Id: hal-03484488**

**<https://hal.science/hal-03484488>**

Submitted on 20 Dec 2021

**HAL** is a multi-disciplinary open access archive for the deposit and dissemination of scientific research documents, whether they are published or not. The documents may come from teaching and research institutions in France or abroad, or from public or private research centers.

L'archive ouverte pluridisciplinaire **HAL**, est destinée au dépôt et à la diffusion de documents scientifiques de niveau recherche, publiés ou non, émanant des établissements d'enseignement et de recherche français ou étrangers, des laboratoires publics ou privés.



Distributed under a Creative Commons Attribution - NonCommercial 4.0 International License

# Optimisation of fast quantification of fluorine content using handheld LIBS

Y. Foucaud<sup>1,\*</sup>, C. Fabre<sup>1,\*</sup>, B. Demeusy<sup>1</sup>, I.V. Filippova<sup>1,2</sup>, L.O. Filippov<sup>1,2</sup>

<sup>1</sup>Université de Lorraine, CNRS, GeoRessources laboratory, F54000 Nancy, France.

<sup>2</sup>National University of science and technology MISIS, 119049 Moscow, Russia

\*Corresponding authors: [yann.foucaud@univ-lorraine.fr](mailto:yann.foucaud@univ-lorraine.fr), [cecile.fabre@univ-lorraine.fr](mailto:cecile.fabre@univ-lorraine.fr)

## Abstract

Hydrofluoric acid represents the majority of the industrial applications of fluorine in the world. It is synthesized from fluorite, which is commonly purified by the froth flotation process to attain the high-grades required for hydrofluoric acid production. Besides, in metallic ores such as tungsten and phosphate ores, fluorite does not represent any added value compared to the extracted metals and is, therefore, considered as a gangue mineral that has to be rejected. In both cases, the fluorine content has to be known precisely in the flotation process as well as in all the industrial applications involving fluorine, to estimate the process efficiency and to optimise the operations. Nevertheless, fluorine quantification is difficult using conventional techniques since it usually includes heavy sample preparation such as dissolution. Though, Laser-Induced Breakdown Spectroscopy (LIBS) provides a multi-element detection that has been successfully used to quantify fluorine using either elementary or CaF molecular bands. Here, rock samples exhibiting a wide range of fluorine contents (from 1.48% to 40.73%) were analysed, the fluorine being mainly comprised in fluorite. These samples corresponded to the products of different flotation tests conducted on the same tungsten-skarn ore. The experimental conditions were optimised to study the two CaF molecular bands, located between 529 and 543 nm, and between 590 and 606 nm, respectively. Systematically, the LIBS emission intensities of the two studied bands were evaluated using the peak areas, which were normalised, averaged over several ablated zones, and correlated with the fluorine content determined by the fluoride-ion sensitive

electrode method. The particle size played a key role as significant differences in the LIBS intensities were exhibited between the 10-150  $\mu\text{m}$  and the  $<20 \mu\text{m}$  powders, with no discernible correlation between the size ranges and signal magnitude. Furthermore, the matrix effects strongly impacted the LIBS intensities, which displayed a non-linear relationship with the fluorine contents: this induced the development of non-linear univariate models that were calculated on 27 training samples and validated on nine testing samples (3:1 ratio). Although non-linear models fitted adequately the experimental data, a multivariate approach considering the two studied CaF bands was adopted to overcome the matrix effects. A formula with linear, quadratic, and interaction terms was generated from the multivariate regression, predicting fluorine contents with  $R^2 = 0.94$  and a mean average error of 2.18 %F. The developed models demonstrated that a precise and accurate quantification of fluorine is possible using a calibrated handheld LIBS, providing an on-line estimation of the processes efficiency and a real-time adaptation.

## Keywords

LIBS; CaF; particle size; molecular bands; normalisation with total light; non-linear models; multivariate modelling;

## 1. Introduction

Fluorite ( $\text{CaF}_2$ ) represents the most important source of fluorine (F) used in the worldwide industry [1–3]. Its main application is the production of hydrofluoric acid (HF) that constitutes the basis of all the fluorine-derivative chemical products (fluoropolymers, fluorocarbon...) [2–5]. Among the fluorine-based chemicals, some are crucial for the industry such as aluminium fluoride ( $\text{AlF}_3$ ), which is essential for the production of metallic aluminium by electrolysis [2,3,6]. Fluorite has many other applications under its mineral form, *e.g.* in the glass industry, for ceramic production [2,3], for epitaxial thin film growth [7], or for the production of ionic superconducting materials [8]. Considering its high economic importance, fluorite has been classified as a Critical Raw Material in the European Union [9].

Most of the fluorite industrial applications require high  $\text{CaF}_2$  grades, making mandatory **its purification by rejecting** the associated gangue minerals. This **concentration** is commonly performed by the froth flotation method **using** fatty acids as collectors [10–15], **which allow** to process low-grade and fine-grained ores. Besides, metallic ores can comprise high amounts of fluorite, which is considered as a by-product that does not bring any added value compared to the extracted metals [16–19]. **Additionally, fluorine** is a penalizing element for the metal-hosting minerals concentrates since it dilutes the metal and produces fluoride ions during the hydrometallurgy stage undergone by the flotation concentrates. Hence, the fluorite elimination from the process is required prior to the hydrometallurgy stage, mainly achieved by the froth flotation technique. This step has become crucial over the past decades as many deposits containing tungsten and phosphate, which have also been classified as Critical Raw Material [9], comprise fluorite as a gangue mineral [16–18].

During the flotation stage of fluorite-containing ores, quantifying the fluorine content in the flows is a key point to assess the performances of the process, *i.e.* the fluorite concentration or elimination, at both laboratory and industrial scales. A fast and efficient on-line fluorine quantification allows to adapt as fast as possible the operating parameters to maintain the product specifications [20]. Several methods have been intensively described for fluorine quantification such as the use of fluoride-ion sensitive electrode (ISO 5439:1978) or the spectrometric measurement of the absorbance (ISO 5438:1993) [21–23]. Fluorine quantification is also possible by ICP-OES/ICP-MS provided that polyatomic ions such as  $\text{BaF}^+$  are formed to decrease the first ionization energy [23,24]. A few other methods exist for fluorine quantification [23] such as liquid/ionic chromatography. However, all the aforementioned methods require time and the use of reagents to dissolve completely fluorite and, then, cannot be employed for fast on-line quantification.

Hence, **either non-destructive methods or techniques requiring no sample preparation are much more adapted for the fast and on-line fluorine quantification issue.** Some authors demonstrated the efficiency of the neutron activation method on rocks [23,25–28], which involves the bombardment of the sample by neutrons produced in the nuclear disintegration of  $^{16}\text{N}$  [27,28]. Nevertheless, this technique is very difficult to use *in situ* due to the intense radioactivity that is produced. Besides,

fluorine content can be measured using elementary or molecular bands of CaF by LIBS (Laser Induced Breakdown Spectroscopy), which is known for not requiring any sample preparation, for its multi-element detection, and for the existence of handheld apparatus that can be used *in situ*. The fluorine quantification by LIBS has been successfully achieved with low limit of detections [29–33], whilst the atmosphere may play a key role [34–36]. However, the primary (and usually the most efficient) emission lines of fluorine are found in the ultra-violet and visible-ultra-violet ranges [30,37–39] in which our spectrometer is not optimised. To address this spectral issue, the detection of the molecular bands that result from the recombination of atomic species in the plasma during cooling has been suggested by previous studies [39–41]. For instance, the measurement of the emission of CaF molecular bands has been intensively investigated and can be used successfully for fluorine quantification [29,31,37,42–44]. However, most previous works [39–41] were based on samples comprising only quartz and fluorite, which is a rare case in the mining area and far from our own case study; thus, we decided to develop both univariate and multiple models to predict the fluorine content of a complex rock sample as a function of the LIBS intensity.

In this work, the measurement of the emission of two different CaF molecular bands using handheld LIBS technique is evaluated for the fluorine quantification on 36 pressed powder pellets coming from various flotation tests, displaying a wide range of fluorine contents. The influence of the particle size is assessed and several models are developed to strengthen quantification models based on statistical methods.

## 2. Materials and methods

### a. Samples

The 36 rock powders analysed in this work were floated and non-floated products from lab-scale flotation experiments performed on the Tabuaço (Northern Portugal) tungsten-skarne. This ore contained fluorite (CaF<sub>2</sub>), scheelite (CaWO<sub>4</sub>), and various silicates among which some are calcic (Figure 1) [45]. Fluorine was mainly hosted by fluorite though the mineralogical characterisation allowed to identify small amount of fluorapatite [Ca<sub>5</sub>(PO<sub>4</sub>)<sub>3</sub>F] and a total substitution of HO<sup>-</sup> by F<sup>-</sup> in hydrated silicate minerals as vesuvianite [45]. Scheelite was finely disseminated and closely

associated with fluorite and vesuvianite (Figure 2), making the flotation mandatory to produce a marketable scheelite concentrate. The 36 samples corresponded to different schemes tested to eliminate fluorite from scheelite concentrates and then displayed fluorine contents ranging from 1.48% to 40.75%.

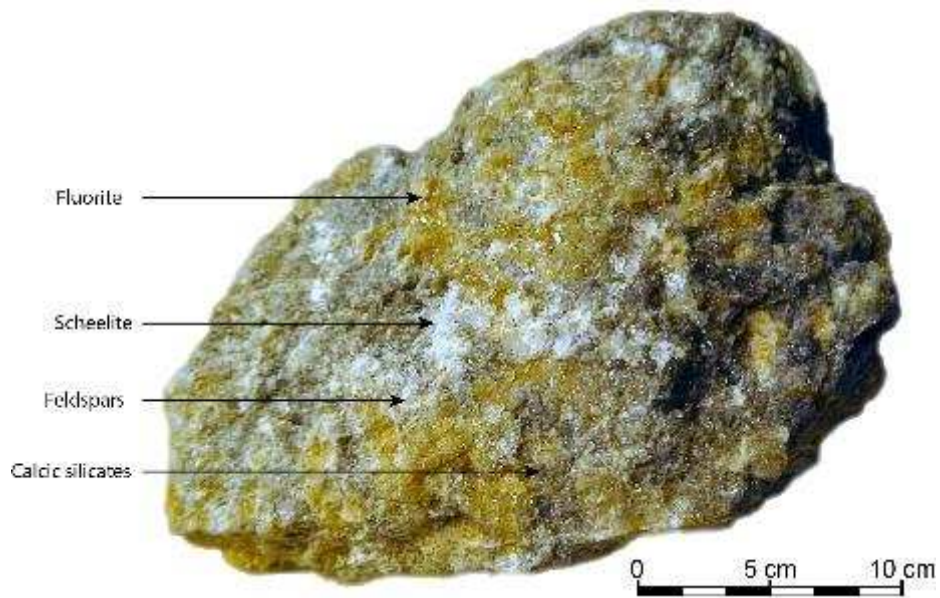


Figure 1. Photograph of the run of mine Tabuaço tungsten skarn displaying mineralogical associations between scheelite, fluorite, and silicates (calcic or not).

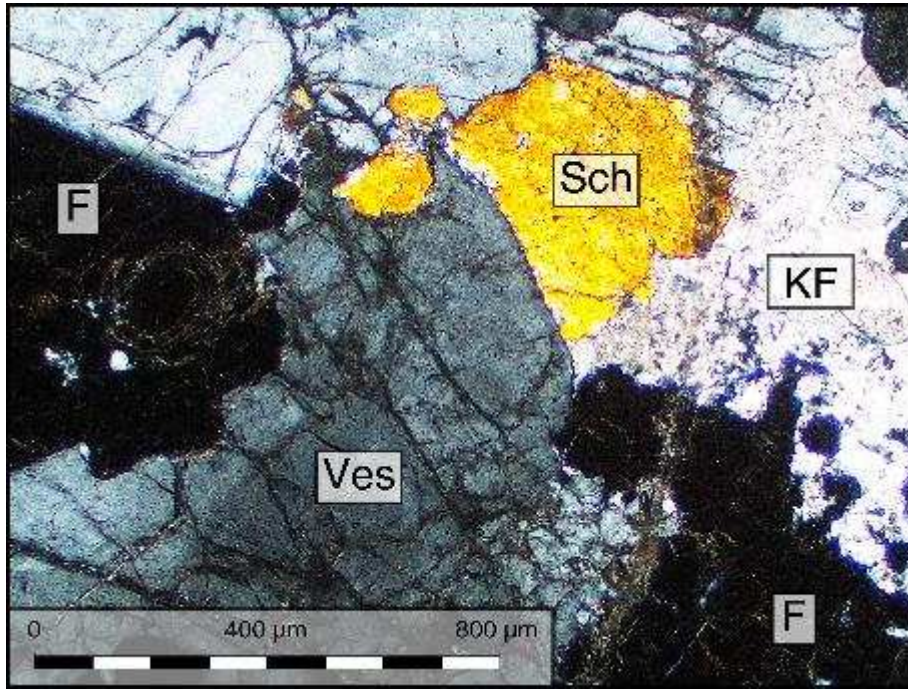


Figure 2. Photograph of the Tabuaço tungsten skarn observed with optical microscope under cross-polarized light, exhibiting its mineralogical associations. Sch = Scheelite ( $\text{CaWO}_4$ ); F = Fluorite ( $\text{CaF}_2$ ); KF = Potassic feldspars; Ves = Vesuvianite (a calcic silicate).

b. Size particle analyses

To estimate the influence of the particle size of the samples in the models, the particle size distribution (PSD) was analysed for each sample by laser light scattering. The obtained PSD were the average of 5 duplicate analyses, which were performed using a Helium-Neon Laser Optical System Mastersizer 3000. The PSD, which is a function, was assessed by a unique value, the  $d_{80}$ , which corresponds to the size that 80% of the particles are finer than.

c. Fluorine analyses

The actual fluorine content of the samples was measured by potentiometric analyses (SARM-CNRS). The products, corresponding to a +150-10  $\mu\text{m}$  fraction, after flotation, were completely dissolved in acidic medium with different sorts of acids. The symbols + and – mean “coarser than” and “finer than”, respectively: a -150+10  $\mu\text{m}$  powder is a ground ore which grains are smaller than 150  $\mu\text{m}$  and coarser than 10  $\mu\text{m}$ . Then, the analyses consisted in the use of a fluoride-ion sensitive electrode (ISE)

which measured the potential of the solution. The error on the F contents with this method was  $\pm 5\%$  of the given value.

#### d. LIBS analyses

Froth flotation was performed on a  $-150+10\ \mu\text{m}$  fraction, corresponding to the ground and deslimed Tabuaço ore. After the flotation tests, the non-floated and floated products were milled in a ring mill to obtain a  $<20\ \mu\text{m}$  fraction, usually used for spectrometric analyses. However, among the 36 samples studied here, 13 were randomly selected and analysed prior to the ring-milling stage in order to assess the influence of the particle size on the LIBS intensities.

For each sample, a representative aliquot of  $1 \pm 0.2\ \text{g}$  of powder was sampled and compacted into a 2-millimeters-thick pellet with a basis pressure of  $6.5\ \text{ton cm}^{-2}$  since some authors demonstrated that the applied compressive force impacts significantly the LIBS intensities below  $3\ \text{ton cm}^{-2}$  [46]. The pellet was then placed under the analysis window of a Sci-Aps © Z-300 handheld LIBS analyser. This analyser displays multiple CCD based spectrometers covering a complete spectral range of 190 nm - 950 nm allowing the record of neutral F emission lines along with CaF molecular bands. The laser power was around 5-6 mJ per pulse (at 50 Hz, 1064 nm) for all the analyses but could display variations of 15%. The ablation craters observed on powder pellets were estimated of 100 micrometres in diameter.

All of the LIBS analyses were performed under a constant argon flow controlled directly by the LIBS handheld instrument with an argon purge displaying a pressure of around 12 psi. Argon atmosphere is known to enhance the emission intensities and minimise the effect of air on the LIBS signal (here 10 times higher). Spectral data can be collected in either ungated or gated operation, with user settable gate delays. Here, concerning the temporal conditions of the plasma analysis, the delay time for the beginning of the acquisition of the LIBS emission was 400 ns. Thus, in order to record the molecular emission of CaF, the acquisition time window was fixed to 1 ms.

For each pellet, the automatic raster mode has been used while the distance between the ablated zones and the distance to the border of the window was optimised to avoid any problem for the plasma

expansion. Nine ablated zones were defined on **three** lines, with **four** zones per line for the two upper lines and **one zone** for the **lower line**, as presented in Figure 3. The ablated zones were separated by 40  $\mu\text{m}$  from each other to avoid any overlapping of craters and, on each zone, **four** laser shots were done, which consisted of a first cleaning shot and 3 successive LIBS analyses (Figure 3).

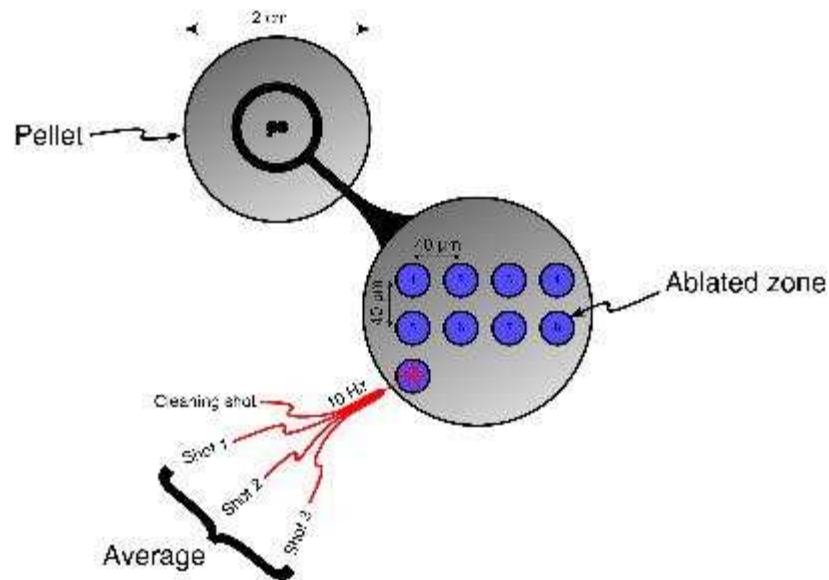


Figure 3. Experimental protocol used for fluorine quantification on pellets with the handheld LIBS raster mode

e. Post-processing

Spectragryph 1.2.9 software was used for the spectra processing [47]. For each analysis, an **automated** method was configured to measure the peak area under the 529-543 nm and 590-606 nm bands **with a baseline to minimize the influence of the background signal. A peak area normalisation with respect to the total light followed by an average of the peak areas over the nine ablated zones for each sample was then applied (report to section 3.c for deeper details).**

The JMP<sup>®</sup> statistical software (SAS institute) was systematically used to build the univariate and multivariate models. For univariate non-linear models, a Newton algorithm [48–50] was used for the gradient convergence, with a convergence criterion of 0.00001. For the model assessment, the  $R^2$ , root

mean squared error (RMSE), and mean absolute error (MAE) were used, which are defined in equations (1), (2), and (3), respectively:

$$R^2 = 1 - \frac{\sum_{i=1}^n (y_i - \hat{y}_i)^2}{\sum_{i=1}^n (y_i - \bar{y})^2} \quad (1)$$

$$RMSE = \sqrt{\frac{1}{n} \sum_{i=1}^n (y_i - \hat{y}_i)^2} \quad (2)$$

$$MAE = \frac{\sum_{i=1}^n |\hat{y}_i - y_i|}{n} \quad (3)$$

where  $y_i$  represents the observed values,  $\hat{y}_i$  the values predicted by the models, and  $\bar{y}$  the mean of the observed values. In equation 1, the numerator represents the sum of squared errors (SSE) while the denominator corresponds to the total sum of squares (TSS). Moreover, an analysis of variance (ANOVA) was performed to assess the significance of each model, through the F-test, with a 0.05 significance level.

### 3. Results

#### a. LIBS analyses

A typical LIBS emission spectrum of a sample with a fluorine content of 14.73% (moderate value) is presented in Figure 4. The delay time to the laser shot and the time gate window were respectively 400 ns and 1 ms, allowing the detection of CaF molecular bands [29,30,42]. Even using these specific parameters, the fluorine atomic emission lines (677.4 nm, 683.4 nm, 685.6 nm, 687.0 nm, 690.2 nm, 691.0 nm, and 696.6 nm), were not detected on the LIBS emission spectra for the entire set of samples (Figure 4, [29,30,51,52]). Although the F atomic emission lines were previously successfully used for fluorine quantification [30,31], their emissions were not sufficient high for low F contents [30], inducing that their peak area could not be measured accurately. Due to a lower ionization potential of the CaF molecule compared to the F element, the optical emission of the CaF molecular bands are stronger than the emission of F atomic lines [29,30,37,42,43]. Since all of the analysed rocks had

significant amounts of calcium and fluorine, their recombination as CaF molecules into the plasma were highly probable using temporal resolution. Hence, to quantify efficiently fluorine on a wide range of fluorine contents, only the CaF molecular bands were considered in this work. The spectral domain ranging between 500 nm and 650 nm, see Figure 4b, contains both the atomic and molecular bands involving Ca atoms. In this domain, the narrow lines peaking at 524.5 nm, 549.0 nm, 556.5 nm, 586.9 nm, and 612.6 nm are ascribed to the Ca I emissions [29–31,37,52]. The large band peaking between 529 and 543 nm is attributed to the  $B^2\Sigma-X^2\Sigma$  system of the CaF molecule while the large bands peaking at 578-585 nm, 590-606 nm, and 616-625 nm are related to the  $A^2\Pi-X^2\Sigma$  system of the CaF molecule [29,53,54]. However, the band peaking between 616 and 625 nm can also be attributed to the CaO molecule while the band peaking between 578 and 585 nm overlaps with a Ca I emission lines [29,55]. Therefore, these two latter bands were not considered in the present study. The intensities of the two other CaF molecular bands were significant for all the samples studied hereby, with fluorine contents ranging from 1.48% to 40.75%. Hence, these bands, peaking at 529-543 nm (green in Figure 4b) and at 590-606 nm (purple in Figure 4b), were selected and used for fluorine content calibration. The use of two separate bands allowed to strengthen the correlation obtained between the peak emission areas and the measured fluorine contents. Also, it enabled the use of a statistical approach to strengthen the results and improve the correlations between LIBS experimental data and actual fluorine contents.

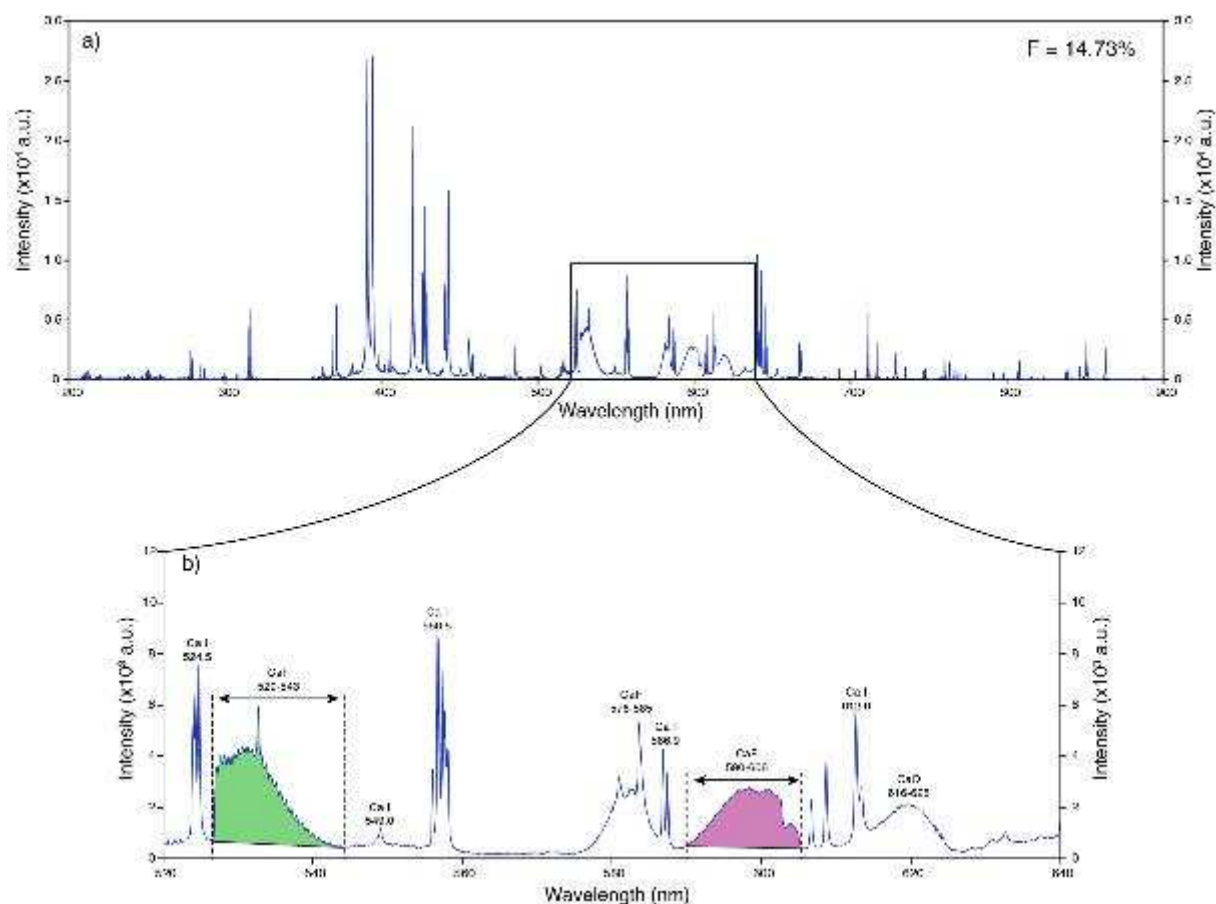


Figure 4. LIBS emission spectrum of a random analysed sample assaying 14.73% F (a) and a zoom on the studied spectral domain ranging from 520 to 640 nm that contains the Ca I atomic lines, the CaO and the CaF molecular bands (b) The areas in green and purple of CaF molecular bands are those used for the spectral ranges and their baselines in the calibration of the fluorine content.

#### b. Influence of the particle size of the powdered pellets

One of the benefits offered by the LIBS analysis done by a handheld tool is the possibility to perform on-line measurements for fluorine quantification all along the process. In this case, the analysed powders would flow from one separation process to another in the plant and would not be milled down to 20  $\mu\text{m}$  prior to the measurement as it was the case for the present work. Hence, it is of paramount interest to assess the influence of the particle size on LIBS emission efficiency.

As mentioned previously, among the 36 samples analysed in this study, 13 were randomly selected and analysed before being milled in the ring mill, their size being then theoretically  $-150+10 \mu\text{m}$ . For those 13 samples, the CaF peaks areas were then measured before and after the milling stage.

Moreover, the particle size distributions of the powders were measured by laser light scattering, providing the  $d_{80}$  values before and after the milling stage. For each of the 13 samples, the ratio of the normalised peak areas,  $Q$ , was calculated using:

$$Q = \frac{NPA_{after\ milling}}{NPA_{before\ milling}} \quad (3)$$

where NPA is the normalised peak area. A  $Q > 1$  corresponds to an increase of the LIBS intensity after the milling stage. For each CaF band,  $Q$  was drawn as a function of the  $d_{80}$  of the powder before the milling stage and the same powder after the milling stage, for the 13 considered samples (Figure 5). No correlation was observed between the normalised peak areas ratio,  $Q$ , the milling ratio, and the  $d_{80}$  of the powder prior to the milling stage, for the two studied molecular bands. However, the milling stage increased significantly the peak areas, *i.e.* the LIBS intensities, since  $Q$  was always higher than 1. Thus, even if no specific grain size is required for the LIBS analysis, the  $d_{80}$  should be roughly the same for all the samples. Therefore, the milling stage, usually performed prior to all spectroscopic analyses, is not necessary for fluorine quantification with a handheld LIBS except if the maximization of the LIBS intensities is needed, *e.g.* when samples exhibit very low fluorine contents.

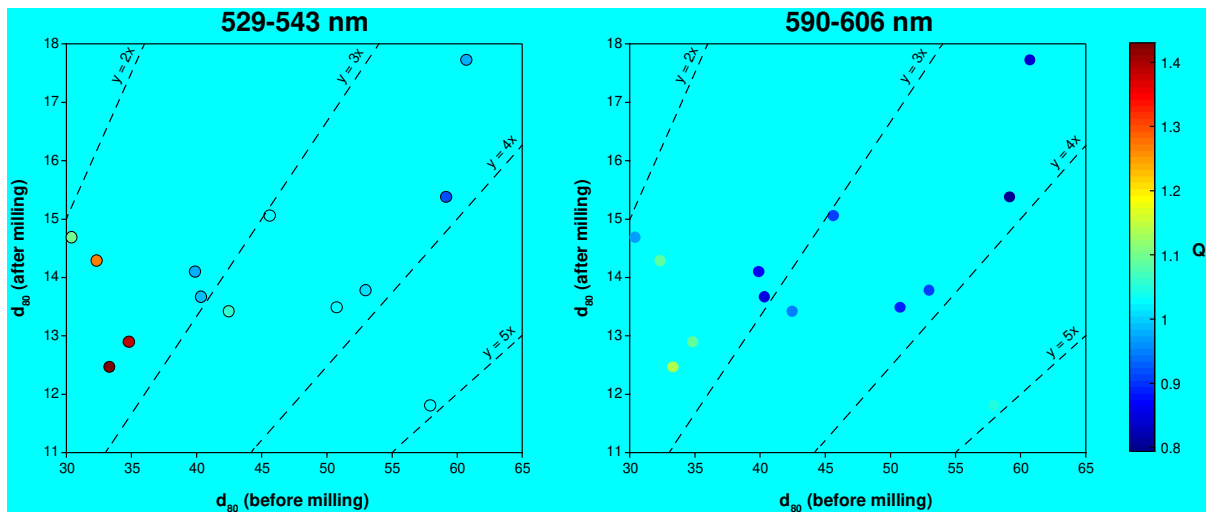


Figure 5. Ratio of the normalised peaks areas before and after milling ( $Q$ , represented by the colour of the points) as a function of the  $d_{80}$  of the powder before milling (x axis) and the  $d_{80}$  of the powder after milling (y axis) for the 529-543 nm (left) and the 590-604 nm CaF (right) bands. The dashed lines represent the milling ratios, corresponding to the  $d_{80}$  before milling divided by the  $d_{80}$  after milling.

### c. Influence of the ablated zones: averaging and normalising

The LIBS apparatus used in this study performed analyses on **nine** ablated zones for each pellet as presented in Figure 3. However, looking carefully zone to zone, we noticed that the **non-normalised** CaF peaks areas differed **significantly** between the **nine** ablated zones. For example, the 529-543 nm peak areas as a function of the actual fluorine contents for each ablated zone are presented in Figure 6. The points density was calculated on the whole domain using a smoothing kernel density algorithm [56,57] and iso-response curves of the points density **provided** the dispersion of the values. **The ablated zones number 2, 3, 4, and 5 exhibited dispersions significantly lower than the first ablated zone (1)** or than the last 4 zones (6, 7, 8, and 9). This could be attributed to some bias on the apparatus (small change in the laser power, argon flow on the sample...) since the pellets were homogeneous in terms of particle size and composition. Each analysed zone was relevant of various grains, since the grain size was around 10  $\mu\text{m}$  for **a <20  $\mu\text{m}$**  product and the laser spot size was around 100  $\mu\text{m}$  in diameter.

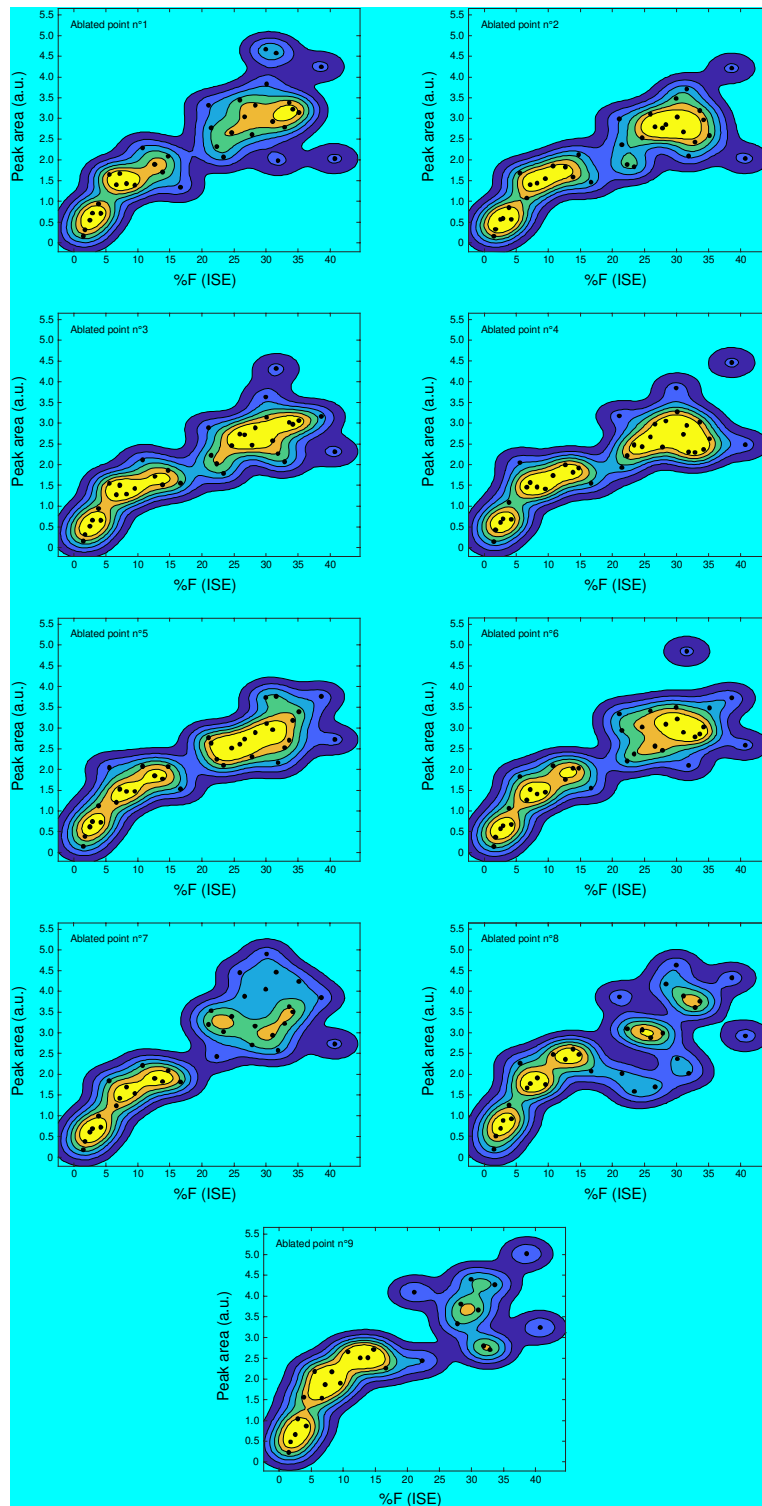


Figure 6. Non-normalised 529-543 nm molecular band areas as a function of the fluorine contents measured by ISE for each ablated zone done using three laser shots after one laser shot cleaning. The coloured contours represent the iso-response curves of the kernel density function; the blue area corresponds to a low point density, the yellow area to a high point density.

Based on these observations, two methods were applied to decrease the peak areas dispersion and to strengthen the models developed on these experimental data. First, for each pellet, the peak areas were averaged on the nine ablated zones following the widely described averaging method [58]. However, the dispersion of the values was still high although it was significantly better than for the nine ablated zones studied separately (Figure 7a); to decrease the dispersion, a normalisation with respect to total light (NTL) was applied to each of the nine spectra, *i.e.* the areas of the two CaF bands were normalised with the whole spectrum area (total light). This technique has been successfully applied in previous studies [59–61] and allows to normalise LIBS emission spectra or peak areas without internal standards, which can vary from one sample to another. Also, for each sample, the nine normalised peak areas, corresponding to the nine ablated zones, were averaged following the classical method [58]. Overall, combining the two methods decreased significantly the dispersion of the values (Figure 7b).

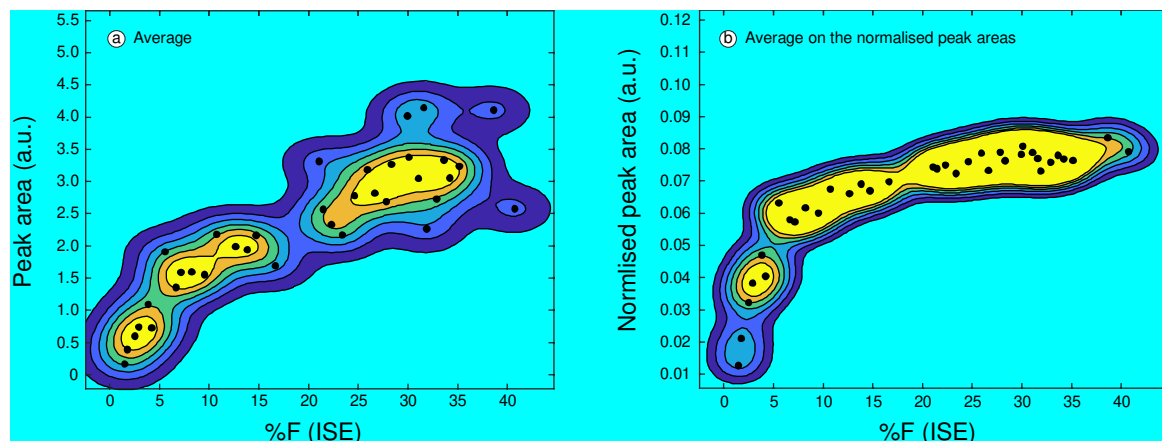


Figure 7. a. Non-normalised 529-543 nm molecular band areas averaged on the nine ablated zones for each pellet as a function of the fluorine contents measured by ISE. b. 529-543 nm molecular band areas averaged over the normalised peak areas of the nine ablated zones for each pellet as a function of the fluorine contents measured by ISE. The coloured contours represent the iso-response curves of the kernel density function; the blue area corresponds to a low point density, the yellow area to a high point density.

#### d. Training and testing samples

Prior to the modelling, the 36 samples analysed by LIBS and ISE were divided in training and testing samples, following the usual procedure for calibration development [62]. The training samples were used for the model development while the testing samples were excluded from the modelling process to validate the models after their development. Among the 36 samples, nine were randomly selected as testing samples and the 27 remaining samples were used for the model development (Table 1). This represented a 3:1 ratio between the training and the testing samples, which is commonly recommended for calibration by authors [62].

Table 1. Sample number and fluorine content measured by ISE of the nine samples randomly selected as testing samples and then excluded from the modelling process.

N° sample	%F (ISE)
2	1.76
5	3.85
10	8.23
15	14.73
16	16.65
21	24.62
27	30.09
33	34.2
34	35.15

#### e. Fluorine quantification using univariate models

Tables S1 and S2 (in SI) regroup sample numbers, fluorine contents measured by ISE, non-normalised and normalised peak areas of the two CaF molecular bands for each ablated zone, and their average over the nine ablated zones. Based on the experimental results, the CaF peak area for the 529-543 nm

peak, in arbitrary unit, was expressed as a function of the fluorine content measured by ISE, as presented on Figure 8. For each sample, the peak areas were the average calculated over the normalised spectra of the nine ablated zones. On Figure 8, the vertical demi error bars correspond to the standard deviation of the normalised peak areas calculated over the nine ablated zones. The horizontal demi error bars represent the experimental error made by the ISE method, which is 5% of the measured fluorine content. The univariate models were developed considering fluorine contents as x values and normalised peak areas as y values, which impels to use invertible functions since the global objective was to predict fluorine content of a sample based on its normalised peak area. Overall, the values followed a non-linear trend (Figure 8) that could be attributed to the formation of other molecules in the plasma, involving either Ca or F atoms, for high CaF<sub>2</sub> contents. Indeed, scheelite, apatite, calcium silicates, and fluorite exhibit similar floatability [63–65], inducing that high fluorine contents, *i.e.* high CaF<sub>2</sub> contents, is correlated with high Ca, P, W, and even Si contents. Hence, at high CaF<sub>2</sub> contents, a part of Ca or F atoms could be used for the formation of MgF or CaO, resulting in a decrease of the CaF content in the plasma. This non-linear trend could be first modelled by a logarithmic model (Figure 8a); since the logarithm function is not defined in zero, a linear horizontal translation was applied by adding a constant value in the logarithm that was also adjusted during the modelling process. This allowed to constraint the model to the origin, *i.e.* to obtain a fluorine content of zero when the normalised peak area was zero. This model fitted the experimental data with  $R^2 = 0.8907$ , a  $p$ -value < 0.0001, a RMSE = 4.2056 %F, and a MAE = 3.1653 %F when the model was inversed to express the fluorine content as a function of the peak area (Table 2). Besides, the asymptote for high fluorine contents also suggested the use of a reciprocal function (Figure 8b), which fitted the experimental data with  $R^2 = 0.8492$ , a  $p$ -value < 0.0001, a RMSE = 4.9390 %F, and a MAE = 3.4855 %F when the model was inversed. This model exhibited significantly lower  $R^2$  and higher RMSE/MAE, which could be attributed to the difficulty to fit correctly the experimental data for both low and high fluorine contents. Due to the asymptote, the errors were very important for high fluorine contents when the model fitted correctly to low fluorine contents while the predicted values for low fluorine contents were negative when the high fluorine content were acceptably predicted, which was not affordable. Overall, the use of the reciprocal function was not suitable for predicting the

fluorine contents from the 529-543 nm normalised peak areas. Finally, a last univariate model was suggested based on the global trend of the values, which were strictly increasing on the studied domain despite an asymptotic behaviour for high fluorine contents (Figure 8c). This was close to a Michaelis-Menten trend, which is a model commonly used to describe enzymatic processes and displays the  $x$  parameter in both the numerator and the denominator of the function. This model fitted the experimental data with  $R^2 = 0.8633$ , a  $p$ -value  $< 0.0001$ , a RMSE = 4.6082 %F, and a MAE = 3.6155 %F when it was inversed, and was, considering the function, constrained to the origin.

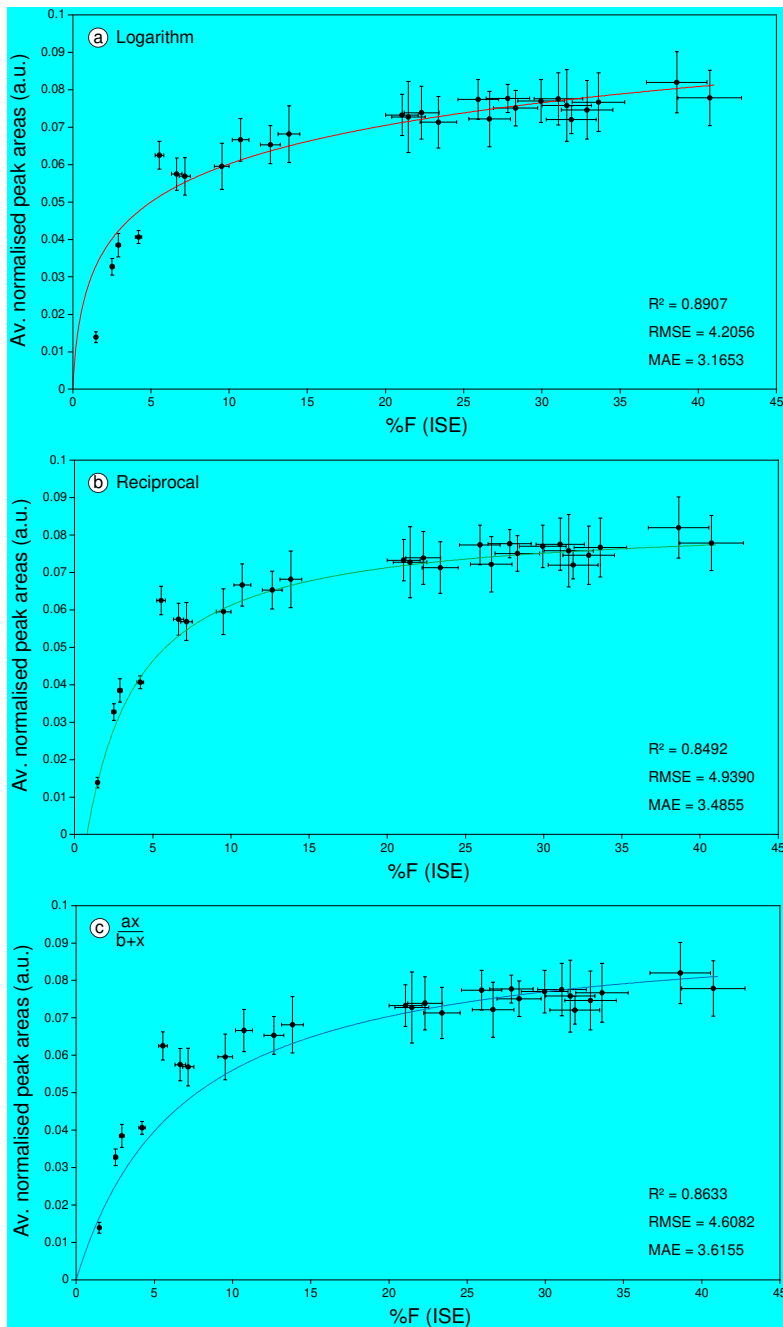


Figure 8. Averages (Av.) normalised peak areas versus fluorine contents measured by ISE, for the 529-543 nm peak presenting the three different univariate models and their summary of fit. The models presented here are all significant ( $p$ -value<0.0001).

Besides, the 590-606 nm peak was studied following a similar procedure. However, the moderate to high fluorine contents displayed constant peak areas, inducing a strong asymptotic behaviour of the curve and, then, the impossibility to inverse the function and to predict the fluorine contents from the LIBS peak areas. The comparison between non-normalised and normalised averaged peak areas

(Figure 9) indicates that the normalisation process was responsible for this asymptotic trend since, without normalisation, a power model could fit the experimental data with  $R^2 = 0.6224$ , a  $p$ -value  $< 0.0001$ , a RMSE = 7.6587 %F, and a MAE = 5.7610 %F when the model was inverted. Overall, the 590-606 nm was very difficult to use for fluorine quantification since non-normalised data exhibited high dispersions while normalised data displayed a strong asymptotic behaviour which made unlikely the modelling process.

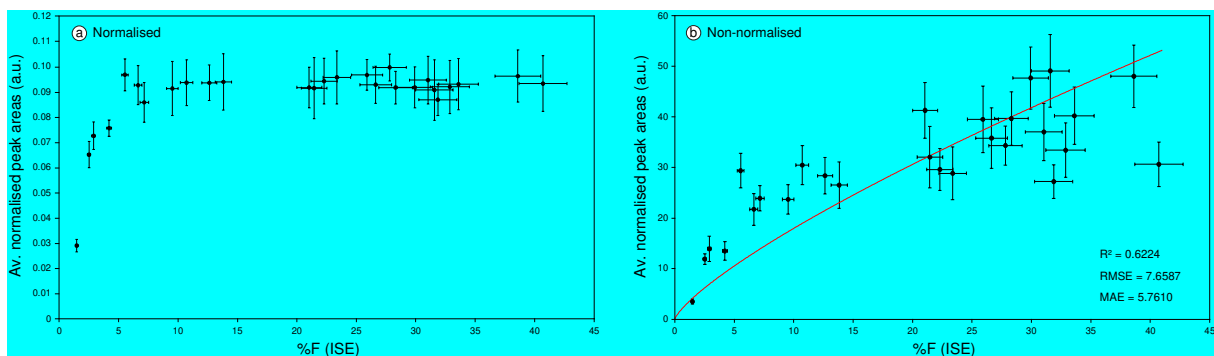


Figure 9. Normalised (a) and non-normalised (b) peak areas averaged over the nine ablated zones for the 590-606 nm CaF band. For non-normalised values, a power model fitted the experimental data with  $p$ -value  $< 0.0001$ , its summary of fit is given.

Table 2. Summary of the different univariate fitting models for the 529-543 nm and 590-606 nm peaks presenting the equations, R<sup>2</sup>, RMSE, and p-value.

Peak	Model type	Model equation	Fluorine content prediction (inversed model)	R <sup>2</sup>	p-value	RMSE	AAE
	Logarithm	$NPA = 0.025168 + 0.015080 \times \ln(\%F + 0.193241)$	$\%F = \text{Exp}\left(\frac{NPA - 0.025168}{0.015080}\right) - 0.193241$	0.8907	<0.0001	4.2056	3.1653
529-543 nm	Reciprocal	$NPA = \frac{-0.506018}{\%F + 5.323205} + 0.091674$	$\%F = \frac{-0.506018}{NPA - 0.091674} - 5.323205$	0.8492	<0.0001	4.9390	3.4855
	$\frac{ax}{b+x}$	$NPA = \frac{\%F \times 0.094757}{6.923864 + \%F}$	$\%F = \frac{-6.923864 \times NPA}{NPA - 0.094757}$	0.8633	<0.0001	4.6082	3.6155
590-606 nm	Power	$PA = 3.055206 \times \%F^{0.769179}$	$\%F = 0.234102 \times PA^{1.300087}$	0.6224	<0.0001	7.6587	5.7610

The prediction models were also compared using the mean absolute error (MAE), which assesses the error that can be done when the fluorine content is predicted (Table 2). The best performance for univariate fluorine quantification was obtained by the logarithmic model, which provided a MAE = 3.1653 %F; this indicated that the fluorine content of a sample can be predicted with handheld LIBS with an average error of 3.1652 % on the fluorine value. However, these comparisons were established on the 27 training samples only. Hence, the nine testing samples, excluded from the modeling process, were used to validate the univariate models by calculating the same indicators than previously, *i.e.* R<sup>2</sup>, RMSE, and MAE (Table 3). Overall, the univariate models predicted correctly the fluorine contents since, on the nine validation samples, the R<sup>2</sup> and MAE were similar or better than on the 27 training samples.

Table 3. Summary of the development and validation of the different univariate fitting models for the 529-543 nm and 590-606 nm peaks presenting, for each model, R<sup>2</sup>, RMSE, and AAE calculated on the 27 training samples and on the nine testing samples.

Peak	Model	Training samples (27)			Testing samples (9)		
		R <sup>2</sup>	RMSE	AAE	R <sup>2</sup>	RMSE	AAE
529-543 nm	Logarithm	0.8907	4.2056	3.1653	0.8875	4.0503	3.0384
	Reciprocal	0.8492	4.9390	3.4855	0.8428	4.7877	3.2748
	$\frac{ax}{b+x}$	0.8633	4.6082	3.6155	0.8582	4.5481	3.6851
590-606 nm	Power	0.6224	7.6587	5.7610	0.8193	5.1337	4.3256

f. Fluorine quantification by multivariate modelling (MLR)

We demonstrated previously that the particle size affected the LIBS peaks areas, despite no significant relationship. Also, the normalisation affected the modelling part since a univariate model could be developed for the non-normalised 590-606 nm peak areas while no model could fit them when they were normalised. Nonetheless, the univariate models considered each of the 529-543 nm and 590-606 nm CaF molecular bands separately; taking into account a linear combination of the two

bands and their possible interactions could lead to an improvement of the models. Hence, a multivariate modelling has also been considered, taking into account the different parameters influencing the calibration between the actual fluorine contents and the LIBS peak areas. Since the univariate models generated previously involved non-linear terms for the CaF peaks areas, quadratic terms were also included in multivariate models, which were developed following the equation:

$$y = a_0 + \sum_{i=1}^k a_i x_i + \sum_{i=1}^{k-1} \sum_{j=1}^k a_{ij} x_i x_j + \sum_{i=1}^k a_{ii} x_i^2 + \varepsilon \quad (4)$$

where  $x_i$  represents the factors, *i.e.* the 529-543 nm peak area (named PA<sub>529-543 nm</sub> after), the 590-606 nm peak area (named PA<sub>590-606 nm</sub> after), and the  $d_{80}$  of each sample;  $a_0$ ,  $a_i$ ,  $a_{ii}$ , and  $a_{ij}$  are the constant, linear, quadratic, and interaction model coefficients, respectively; and  $\varepsilon$  is a residual. The coefficients and the residual were estimated via the least square method [66–68]. A Student test was realized on each calculated model coefficient with a confidence level of 95% to select the significant coefficients. The analysis of variance (ANOVA) was used to assess the model significance and eliminate the non-significant coefficients from the final models. Multilinear regressions were developed on normalised and non-normalised peak areas to assess the effect of normalisation. Figure 10 presents the correlations between the fluorine contents measured by ISE and the fluorine contents predicted by the multilinear models, on both non-normalised (Figure 10a) and normalised (Figure 10b) peak areas averaged over the nine ablated zones, and gives the  $R^2$ , RMSE, MAE, and  $p$ -value of the final models. Also, Table 4 summarizes the coefficients of the final models, which were all significant with a confidence level of 95%. The linear terms of the two CaF molecular bands, the interaction term between the two CaF molecular bands, and the quadratic terms for the 529-543 nm band were significant (Table 4). The significance of the quadratic terms confirmed the global non-linear trend observed and discussed previously for the univariate models. Furthermore, the coefficients involving the  $d_{80}$  were all non-significant, which confirmed that, although the particle size globally impacted the peak areas, it did not affect significantly the fluorine quantification. It also confirmed that a fluorine quantification using a handheld LIBS is possible with no dependence on the particle size as long as all the samples have roughly the same PSD.

Table 4. Parameter estimates for the final multivariate models as a function of the standardized parameters with standard errors (STD), t-ratios (T), and *p*-values (P), for non-normalised and normalised peak areas.

Term	Estimate	STD error	T	P
<i>Non-normalised peak areas</i>				
Constant	32.81	3.84	8.55	<0.0001
PA <sub>529-543 nm</sub>	6.10	0.52	11.75	<0.0001
PA <sub>590-606 nm</sub>	-5.02	0.51	-9.84	<0.0001
(PA <sub>529-543 nm</sub> - 23.33)*(PA <sub>529-543 nm</sub> - 23.33)	0.15	0.05	3.04	0.006
(PA <sub>529-543 nm</sub> - 23.33)*(PA <sub>590-606 nm</sub> - 30.41)	-0.17	0.05	-3.59	0.0016
<i>Normalised peak areas</i>				
NPA <sub>529-543 nm</sub>	1449.82	88.95	16.30	<0.0001
NPA <sub>590-606 nm</sub>	-880.99	70.23	-12.54	<0.0001
(NPA <sub>529-543 nm</sub> - 0.07)*(NPA <sub>529-543 nm</sub> - 0.07)	29344.53	6236.31	4.71	<0.0001
(NPA <sub>529-543 nm</sub> - 0.07)*(NPA <sub>590-606 nm</sub> - 0.08)	-23412.95	5591.33	-4.19	0.0004

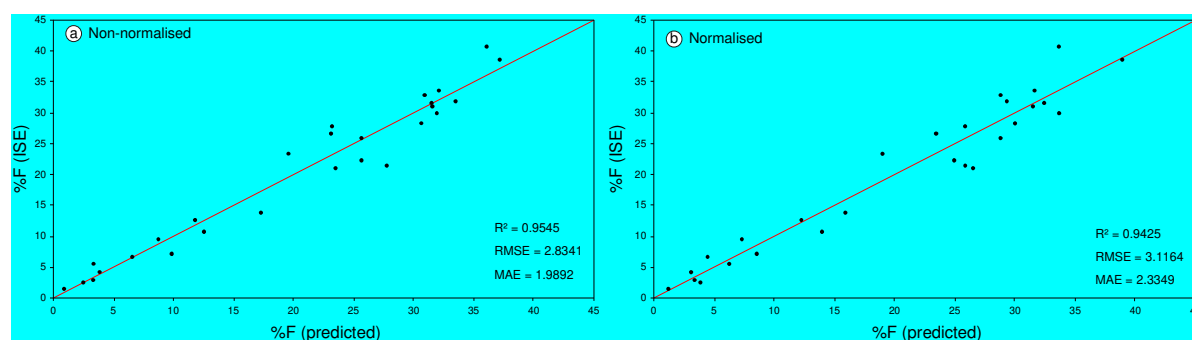


Figure 10. Observed fluorine contents (ISE) expressed as a function of the fluorine contents predicted by the multivariate models developed for normalised (a) and non-normalised peak areas averaged over the nine ablated zones. R<sup>2</sup>, RMSE, and MAE are presented for the two models, which were significant (*p*-value<0.0001). Red lines represent the *y* = *x* curve.

Overall, the multivariate model calculated on non-normalised peak areas exhibited better  $R^2$ , RMSE, and MAE compared to model developed on normalised peak areas, which demonstrated that a normalisation was not necessary to obtain accurate multivariate models (Table 5, Figure 10). The best multivariate model, calculated on non-normalised peak areas averaged over the nine ablated zones of each sample, exhibited  $R^2 = 0.9545$ , a RMSE = 2.8341 %F, and a MAE = 1.9592 %F for a  $p$ -value < 0.0001. As for the univariate models, the multivariate models were validated by predicting the fluorine contents of the nine testing samples (Table 5).

Table 5. Observed and predicted values for the two different multivariate models with the absolute and relative errors along with the correlation and prediction indicators, ( $R^2$ , RMSE, and MAE) calculated on the nine testing samples.

%F (ISE)	Non-normalised peak areas			Normalised peak areas		
	%F (predicted)	Absolute error	Relative error (%)	%F (predicted)	Absolute error	Relative error (%)
1.76	1.86	0.10	5.47	3.93	2.17	123.07
3.85	2.95	0.90	30.48	2.50	1.35	34.99
8.23	10.94	2.71	24.76	8.99	0.76	9.26
14.73	14.98	0.25	1.65	15.30	0.57	3.84
16.65	17.35	0.70	4.06	15.72	0.93	5.56
24.62	22.40	2.22	9.92	24.58	0.04	0.18
30.09	31.24	1.15	3.68	32.83	2.74	9.09
34.2	28.75	5.46	18.98	29.12	5.08	14.86
35.15	28.22	6.93	24.56	29.11	6.04	17.18
<i>Total on testing samples (9)</i>						
$R^2$	0.9293			0.9406		

RMSE	2.0534	1.8833
MAE	2.2687	2.1852

*Training samples (27)*

R <sup>2</sup>	0.9545	0.9425
RMSE	2.8341	3.1164
MAE	1.9892	2.3349

For the nine validation samples, the model with normalised peak areas exhibited slightly better performances, with higher R<sup>2</sup> and lower RMSE/MAE. However, the relative error was significant for the low fluorine contents, which can be attributed to the minimisation of the RMSE that is calculated from the absolute errors. Overall, multivariate models provided a fluorine quantification with handheld LIBS with around 2.2 %F average error for fluorine contents ranging from 1% to 40%, which corresponds to 2% to 80% of CaF<sub>2</sub> contents.

#### 4. Conclusion

The main goal of this work was to develop a fast and accurate fluorine quantification method on powders for a wide range of applications including mineral processing area. To attain this objective, a handheld LIBS was used on 36 samples from flotation tests, containing from 1.48% F to 40.73% F, which fluorine content was measured by ISE. The handheld LIBS ablated nine different zones for each sample and two CaF molecular bands were studied for fluorine quantification. We demonstrated that the particle size had a significant effect on the LIBS intensities with however no correlation. Moreover, we found a variability in the LIBS intensities regarding the different ablated zones of a sample. Hence, for the fluorine quantification, averaging and normalising with respect to the total light were applied to decrease the values dispersion. Also, the 36 samples were randomly divided into 27 training samples and nine testing samples for model development and model validation, respectively. Then, univariate non-linear models were developed on each CaF band studied separately, with

significantly better performances for the 529-543 nm peak. The best univariate model provided a quantification with  $R^2 = 0.8907$  and  $MAE = 3.1653\%F$ , which represented the averaged error that was done on the prediction. Besides, the quantification accuracy was improved using multivariate models that took into account the two studied peaks through a linear term and a quadratic term for both as well as an interaction term. Multivariate models were developed for normalised and non-normalised peak areas to assess the influence of normalisation process. Overall, the best multivariate model, calculated from normalised peak areas, fitted the 27 training fluorine contents with  $R^2 = 0.9425$  and a  $MAE = 2.3349\%F$  and predicted the nine testing fluorine contents with  $R^2 = 0.9406$  and a  $MAE = 2.1822\%F$ . Thus, an on-line LIBS analyser can be set on a  $CaF_2$ -rich sample where 2% of error in absolute value will not impact the process adaptation. The method developed in the present work aims at adapting the process based on on-line analyses but not at analysing the final marketable products, which have to be analysed with certified methods such as ISE. Overall, a fluorine quantification by a handheld LIBS is possible on powders and can be applied in the mineral processing area as in-situ quantification apparatus with a unique condition of a roughly constant particle size. With handheld LIBS, the use of helium as a purge gas could improve the limit of detection as well as the models accuracy and should be studied in details by other studies. Moreover, handheld XRF are now available with graphene windows that can detect and measure fluorine, which could be another route to investigate in the future.

## Acknowledgements

We thank anonymous reviewers for their helpful and wise suggestions and comments, their expertise on the data treatment has been gratefully appreciated. The research leading to these results has received funding from the European Union's Horizon 2020 research and innovation programme under grant agreement No 641650 for the FAME project. We also acknowledge the support of Labex Ressources 21 supported by the French National Research Agency through the national program "Investissements d'Avenir" [reference ANR-10-LABX-21-01]. SciAps © Z300 handheld tool was acquired using the co-financial supports from GISFI-Tech and ICÈEL Institut Carnot.

## References

- [1] J. Emsley, *Nature's building blocks: an A-Z guide to the elements*, New ed., completely rev. and updated, Oxford University Press, Oxford ; New York, 2011.
- [2] J. Féraud, *Mémento des roches et minéraux industriels : la fluorine ou spath fluor* (in french), (1999).
- [3] GOVERNMENT PUBLISHING OFFICE, *MINERAL COMMODITY SUMMARIES 2017.*, U S GOVT PRINTING OFFICE, S.I., 2017.
- [4] M.L. Free, J.D. Miller, Kinetics of 18-Carbon Carboxylate Adsorption at the Fluorite Surface, *Langmuir*. 13 (1997) 4377–4382. doi:10.1021/la960329r.
- [5] R. Sattmann, I. Mönch, H. Krause, R. Noll, S. Couris, A. Hatziapostolou, A. Mavromanolakis, C. Fotakis, E. Larrauri, R. Miguel, Laser-Induced Breakdown Spectroscopy for Polymer Identification, *Applied Spectroscopy*. 52 (1998) 456–461. doi:10.1366/0003702981943680.
- [6] T.R. Beck, R.J. Brooks, *Electrolytic reduction of alumina*, 1989.
- [7] St. Klumpp, H. Dabringhaus, Experimental study of the adsorption of lithium fluoride on the (111) surface of CaF<sub>2</sub>, *Surface Science*. 417 (1998) 323–336. doi:10.1016/S0039-6028(98)00684-0.
- [8] L.N. Patro, K. Hariharan, Fast fluoride ion conducting materials in solid state ionics: An overview, *Solid State Ionics*. 239 (2013) 41–49. doi:10.1016/j.ssi.2013.03.009.
- [9] European Commission, I. Directorate-General for Internal Market Entrepreneurship and SMEs, Deloitte Sustainability, British Geological Survey, Toegest past natuurwetenschappelijk onderzoek, *Study on the review of the list of critical raw materials final report.*, 2017.

- [10] J.A. Mielczarski, E. Mielczarski, J.M. Cases, Dynamics of Fluorite–Oleate Interactions, *Langmuir*. 15 (1999) 500–508. doi:10.1021/la980593f.
- [11] E. Mielczarski, J.A. Mielczarski, J.M. Cases, B. Rai, others, Influence of solution conditions and mineral surface structure on the formation of oleate adsorption layers on fluorite, *Colloids and Surfaces A: Physicochemical and Engineering Aspects*. 205 (2002) 73–84.
- [12] Y. Zhang, S. Song, Beneficiation of fluorite by flotation in a new chemical scheme, *Minerals Engineering*. 16 (2003) 597–600. doi:10.1016/S0892-6875(03)00136-5.
- [13] S. Song, A. Lopez-Valdivieso, C. Martinez-Martinez, R. Torres-Armenta, Improving fluorite flotation from ores by dispersion processing, *Minerals Engineering*. 19 (2006) 912–917. doi:10.1016/j.mineng.2005.10.005.
- [14] D. LIN, G. NIE, G. LUO, Z. TANG, Collect mechanisms of oleic acid on fluorite and calcite minerals, (2016).
- [15] Y. Foucaud, S. Lebègue, L.O. Filippov, I.V. Filippova, M. Badawi, Molecular Insight into Fatty Acid Adsorption on Bare and Hydrated (111) Fluorite Surface, *The Journal of Physical Chemistry B*. 122 (2018) 12403–12410. doi:10.1021/acs.jpcc.8b08969.
- [16] N. Kupka, M. Rudolph, Froth flotation of scheelite – A review, *International Journal of Mining Science and Technology*. 28 (2018) 373–384. doi:10.1016/j.ijmst.2017.12.001.
- [17] R. Houot, Beneficiation of phosphatic ores through flotation: Review of industrial applications and potential developments, *International Journal of Mineral Processing*. 9 (1982) 353–384. doi:10.1016/0301-7516(82)90041-2.
- [18] M. Jébrak, É. Marcoux, M. Laithier, *Geology of mineral resources*, Second edition, Geological Association of Canada, St. John's, NL, 2016.
- [19] X. Yang, Beneficiation studies of tungsten ores – A review, *Minerals Engineering*. 125 (2018) 111–119. doi:10.1016/j.mineng.2018.06.001.

- [20] N. Khajehzadeh, O. Haavisto, L. Koresaar, On-stream and quantitative mineral identification of tailing slurries using LIBS technique, *Minerals Engineering*. 98 (2016) 101–109. doi:10.1016/j.mineng.2016.08.002.
- [21] E01 Committee, Test Method for Determination of Calcium Fluoride in Fluorspar by EDTA Complexometric Titrimetry, ASTM International, n.d. doi:10.1520/E0815-17B.
- [22] D16 Committee, Test Methods for Analysis of Acid-Grade Calcium Fluoride (Fluorspar), ASTM International, n.d. doi:10.1520/E1506-08.
- [23] P.A. Mello, J.S. Barin, F.A. Duarte, C.A. Bizzi, L.O. Diehl, E.I. Muller, E.M.M. Flores, Analytical methods for the determination of halogens in bioanalytical sciences: a review, *Analytical and Bioanalytical Chemistry*. 405 (2013) 7615–7642. doi:10.1007/s00216-013-7077-9.
- [24] N. Yamada, Feasibility study of fluorine detection by ICP-QQQ, Agil. 8800 ICP-QQQ Appl. Handb., Agilent Technologies, 2013, pp. 33–34., (n.d.).
- [25] K. Randle, Determination of fluorine in geological samples using accelerator derived neutrons, *Journal of Radioanalytical and Nuclear Chemistry Articles*. 90 (1985) 355–361. doi:10.1007/BF02060792.
- [26] H.Gene. Knight, A.Keith. Furr, T.F. Parkinson, Determination of fluorine by neutron activation analysis, *Analytical Chemistry*. 49 (1977) 1507–1510. doi:10.1021/ac50019a013.
- [27] M.P. Castro-García, T. Alonso-Sánchez, M.A. Rey-Ronco, Study of the gamma spectrum of  $^{16}\text{N}$  with a BGO detector, for the purpose of calibration and of determining the fluorine grade of mineral samples, *Journal of Radioanalytical and Nuclear Chemistry*. 298 (2013) 915–921. doi:10.1007/s10967-013-2599-3.

- [28] T. Alonso Sánchez, M.A. Rey Ronco, M.P. Castro García, A neutron activation technique for the analysis for fluorine in fluorspar samples, *International Journal of Mineral Processing*. 94 (2010) 1–13. doi:10.1016/j.minpro.2009.11.003.
- [29] M. Gaft, L. Nagli, N. Eliezer, Y. Groisman, O. Forni, Elemental analysis of halogens using molecular emission by laser-induced breakdown spectroscopy in air, *Spectrochimica Acta Part B: Atomic Spectroscopy*. 98 (2014) 39–47. doi:10.1016/j.sab.2014.05.011.
- [30] C. Álvarez, J. Pisonero, N. Bordel, Quantification of fluorite mass-content in powdered ores using a Laser-Induced Breakdown Spectroscopy method based on the detection of minor elements and CaF molecular bands, *Spectrochimica Acta Part B: Atomic Spectroscopy*. 100 (2014) 123–128. doi:10.1016/j.sab.2014.07.024.
- [31] O. Forni, M. Gaft, M.J. Toplis, S.M. Clegg, S. Maurice, R.C. Wiens, N. Mangold, O. Gasnault, V. Sautter, S. Le Mouélic, P.-Y. Meslin, M. Nachon, R.E. McInroy, A.M. Ollila, A. Cousin, J.C. Bridges, N.L. Lanza, M.D. Dyar, First detection of fluorine on Mars: Implications for Gale Crater’s geochemistry: First detection of fluorine on Mars, *Geophysical Research Letters*. 42 (2015) 1020–1028. doi:10.1002/2014GL062742.
- [32] D.A. Cremers, L.J. Radziemski, Detection of chlorine and fluorine in air by laser-induced breakdown spectrometry, *Analytical Chemistry*. 55 (1983) 1252–1256. doi:10.1021/ac00259a017.
- [33] C.D. Quarles, J.J. Gonzalez, L.J. East, J.H. Yoo, M. Morey, R.E. Russo, Fluorine analysis using Laser Induced Breakdown Spectroscopy (LIBS), *Journal of Analytical Atomic Spectrometry*. 29 (2014) 1238. doi:10.1039/c4ja00061g.
- [34] G. Asimellis, S. Hamilton, A. Giannoudakos, M. Kompitsas, Controlled inert gas environment for enhanced chlorine and fluorine detection in the visible and near-infrared

- by laser-induced breakdown spectroscopy, *Spectrochimica Acta Part B: Atomic Spectroscopy*. 60 (2005) 1132–1139. doi:10.1016/j.sab.2005.05.035.
- [35] M. Tran, B.W. Smith, D.W. Hahn, J.D. Winefordner, Detection of Gaseous and Particulate Fluorides by Laser-Induced Breakdown Spectroscopy, *Applied Spectroscopy*. 55 (2001) 1455–1461. doi:10.1366/0003702011953865.
- [36] M. Tran, Q. Sun, B.W. Smith, J.D. Winefordner, Determination of F, Cl, and Br in Solid Organic Compounds by Laser-Induced Plasma Spectroscopy, *Applied Spectroscopy*. 55 (2001) 739–744. doi:10.1366/0003702011952433.
- [37] P. Pořízka, S. Kaski, A. Hrdlička, P. Modlitbová, L. Sládková, H. Häkkinen, D. Prochazka, J. Novotný, P. Gadas, L. Čelko, K. Novotný, J. Kaiser, Detection of fluorine using laser-induced breakdown spectroscopy and Raman spectroscopy, *Journal of Analytical Atomic Spectrometry*. 32 (2017) 1966–1974. doi:10.1039/C7JA00200A.
- [38] D.A. Cremers, L.J. Radziemski, *Handbook of Laser-Induced Breakdown Spectroscopy: Cremers/Handbook of Laser-induced Breakdown Spectroscopy*, John Wiley & Sons, Ltd, Chichester, UK, 2006. doi:10.1002/0470093013.
- [39] J. Papish, L.E. Hoag, W.E. Snee, Spectroscopic Detection of Fluorine, *Industrial & Engineering Chemistry Analytical Edition*. 2 (1930) 263–264. doi:10.1021/ac50071a022.
- [40] O.B. Troshkina, Special features of the use of molecular bands in emission spectral analysis on the basis of fluorine determination data in the CaF band, *Journal of Applied Spectroscopy*. 14 (1971) 430–437. doi:10.1007/BF00616107.
- [41] R.C. Johnson, The Band Spectra of the Alkaline Earth Halides. I. CaF, SrF, *Proceedings of the Royal Society A: Mathematical, Physical and Engineering Sciences*. 122 (1929) 161–188. doi:10.1098/rspa.1929.0012.

- [42] M. Oujja, R. de Nalda, M. López-Arias, R. Torres, J.P. Marangos, M. Castillejo, CaF 2 ablation plumes as a source of CaF molecules for harmonic generation, *Physical Review A*. 81 (2010). doi:10.1103/PhysRevA.81.043841.
- [43] Z.J. Jakubek, N.A. Harris, R.W. Field, J.A. Gardner, E. Murad, Ionization potentials of CaF and BaF, *The Journal of Chemical Physics*. 100 (1994) 622–627. doi:10.1063/1.466923.
- [44] F.R. Doucet, P.J. Faustino, M. Sabsabi, R.C. Lyon, Quantitative molecular analysis with molecular bands emission using laser-induced breakdown spectroscopy and chemometrics, *Journal of Analytical Atomic Spectrometry*. 23 (2008) 694. doi:10.1039/b714219f.
- [45] Y. Foucaud, B. Lechenard, P. Marion, I. Filippova, L. Filippov, Geology, Textural Study, Ore Genesis and Processing of the Tabuaço Tungsten Deposit (Northern Portugal), in: A.I. Al-Juboury (Ed.), *Contributions to Mineralization*, InTech, 2018. doi:10.5772/intechopen.71674.
- [46] A.M. Popov, S.M. Zaytsev, I.V. Seliverstova, A.S. Zakuskin, T.A. Labutin, Matrix effects on laser-induced plasma parameters for soils and ores, *Spectrochimica Acta Part B: Atomic Spectroscopy*. 148 (2018) 205–210. doi:10.1016/j.sab.2018.07.005.
- [47] F. Menges, Spectragryph - optical spectroscopy software", Version 1.2.9, 2018, <http://www.ffmpeg2.de/spectragryph/>, n.d.
- [48] A.F. Izmailov, M.V. Solodov, *Newton-type methods for optimization and variational problems*, Springer, Cham ; New York, 2014.
- [49] P. Deuffhard, *Newton methods for nonlinear problems: affine invariance and adaptive algorithms*, Springer, Berlin ; New York, 2004.
- [50] J. Nocedal, S.J. Wright, *Numerical optimization*, 2nd ed, Springer, New York, 2006.

- [51] J.E. Sansonetti, W.C. Martin, Handbook of Basic Atomic Spectroscopic Data, *Journal of Physical and Chemical Reference Data*. 34 (2005) 1559–2259. doi:10.1063/1.1800011.
- [52] A. Kramida, Y. Ralchenko, NIST Atomic Spectra Database, NIST Standard Reference Database 78, (1999). doi:10.18434/T4W30F.
- [53] M. Peterson, H. Jaffe, Visual arc spectroscopic detection analysis, US Dept. of the Interior, Bur. Mines, Bull, 1953. 524., (n.d.).
- [54] R.W.B. Pearse, A.G. Gaydon, *The Identification of Molecular Spectra*, Springer Netherlands, Dordrecht, 1976. doi:10.1007/978-94-009-5758-9.
- [55] R.M. Dagnall, K.C. Thompson, T.S. West, Molecular-emission spectroscopy in cool flames. Part I. The behaviour of sulphur species in a hydrogen-nitrogen diffusion flame and in a shielded air-hydrogen flame, *The Analyst*. 92 (1967) 506. doi:10.1039/an9679200506.
- [56] M. Rosenblatt, Remarks on Some Nonparametric Estimates of a Density Function, *The Annals of Mathematical Statistics*. 27 (1956) 832–837. doi:10.1214/aoms/1177728190.
- [57] E. Parzen, On Estimation of a Probability Density Function and Mode, *The Annals of Mathematical Statistics*. 33 (1962) 1065–1076. doi:10.1214/aoms/1177704472.
- [58] J.P. Castro, E.R. Pereira-Filho, Twelve different types of data normalization for the proposition of classification, univariate and multivariate regression models for the direct analyses of alloys by laser-induced breakdown spectroscopy (LIBS), *J. Anal. At. Spectrom.* 31 (2016) 2005–2014. doi:10.1039/C6JA00224B.
- [59] V. Karki, A. Sarkar, M. Singh, G.S. Maurya, R. Kumar, A.K. Rai, S.K. Aggarwal, Comparison of spectrum normalization techniques for univariate analysis of stainless steel by laser-induced breakdown spectroscopy, *Pramana - J Phys.* 86 (2016) 1313–1327. doi:10.1007/s12043-015-1180-8.

- [60] Z. Wang, L. Li, L. West, Z. Li, W. Ni, A spectrum standardization approach for laser-induced breakdown spectroscopy measurements, *Spectrochimica Acta Part B: Atomic Spectroscopy*. 68 (2012) 58–64. doi:10.1016/j.sab.2012.01.005.
- [61] C.B. Stipe, B.D. Hensley, J.L. Boersema, S.G. Buckley, Laser-Induced Breakdown Spectroscopy of Steel: A Comparison of Univariate and Multivariate Calibration Methods, *Appl Spectrosc*. 64 (2010) 154–160. doi:10.1366/000370210790619500.
- [62] F. Westad, F. Marini, Validation of chemometric models – A tutorial, *Analytica Chimica Acta*. 893 (2015) 14–24. doi:10.1016/j.aca.2015.06.056.
- [63] I.V. Filippova, L.O. Filippov, A. Duverger, V.V. Severov, Synergetic effect of a mixture of anionic and nonionic reagents: Ca mineral contrast separation by flotation at neutral pH, *Minerals Engineering*. 66–68 (2014) 135–144. doi:10.1016/j.mineng.2014.05.009.
- [64] L.O. Filippov, Y. Foucaud, I.V. Filippova, M. Badawi, New reagent formulations for selective flotation of scheelite from a skarn ore with complex calcium minerals gangue, *Minerals Engineering*. 123 (2018) 85–94. doi:10.1016/j.mineng.2018.05.001.
- [65] Y. Foucaud, I.V. Filippova, L.O. Filippov, Investigation of the depressants involved in the selective flotation of scheelite from apatite, fluorite, and calcium silicates: Focus on the sodium silicate/sodium carbonate system, *Powder Technology*. (2019) S0032591019303195. doi:10.1016/j.powtec.2019.04.071.
- [66] A.M. Dean, D. Voss, *Design and Analysis of Experiments: Springer Texts in Statistics.*, Springer-Verlag New York Inc., Dordrecht, 2003.
- [67] D.C. Montgomery, *Design and analysis of experiments*, Eighth edition, John Wiley & Sons, Inc, Hoboken, NJ, 2013.
- [68] R.H. Myers, D.C. Montgomery, C.M. Anderson-Cook, *Response surface methodology: process and product optimization using designed experiments*, Fourth edition, Wiley, Hoboken, New Jersey, 2016.